CHAPTER VI

HYSTERESIS AND STRAIN HARDENING IN THE CREEP RESPONSE OF A POLYANILINE ER FLUID

6.1 Abstract

The electrorheological creep response of PANI)/silicone oil suspensions near the yield point is investigated using parallel plate rheometry. Controlled-stress, thixotropic loop experiments exhibit a pronounced hysteresis, from which we determined the static yield stress ($\sigma_{y(static)}$), as the stress where onset of flow occurs on the upward part of the loop, and a dynamic yield stress ($\sigma_{y(dynamic)}$), defined as the stress at which flow ceases on the downward part of the loop. The magnitude of the hysteresis, as characterized by the area under the loop, increases substantially with applied field strength and particle concentration, but decreases with increase of temperature. Consistent with literature data, the creep compliance shows an evolution from viscoelastic to viscoplastic to viscous flow behavior as the applied stress increases through the yield point. In the viscoplastic regime, the apparent equilibrium compliance, J_e^{app}, shows a discrete pre-yield transition to higher values, indicating a seemingly-enhanced ductility as the applied stress nears the yield point. Measurement of the static yield stress following these creep experiments suggests that the origin of this transition is a pronounced strain-hardening effect. We conclude that strain-hardening contributes to the hysteresis observed in the thixotropic loop test.

KEYWORDS: Electrorheology, Creep, Conductive polymer, Polyaniline

6.2 Introduction

An electrorheological (ER) fluid typically consists of a suspension of dielectric particles in a liquid of low dielectric constant. The suspension viscosity increases and the suspension undergoes a rapid transition from a Newtonian liquid to a Bingham plastic upon the application of an electric field (Winslow, 1949). This transformation is caused by the formation of internal chain-like structures that are created by the agglomeration of the dispersed particles, polarized by the applied field. The resulting change in viscoelastic properties has been utilized in applications such as shock absorbers, clutches, brakes, actuators, artificial joints and robotic controls (Bohon and Krause, 1998, Papadopoulos, 1998, Akella and Cutkosky, 1995, Choi *et al.*, 1998). It is noteworthy that certain applications, such as active dampers, involve loading conditions below the yield stress or oscillations with small amplitudes, and the Bingham plastic assumption, which works reasonably well for high strain rates, does not accurately describe the fluid behavior at small strain rates below the yield point (Kamath and Wereley, 1997). Thus, creep experiments are useful to gain insight into the deformation mechanisms of the solid structure associated with the yield transition (Otsubo and Edamura, 1994). Polyaniline is a conducting polymer which has been used to form the dispersed particles in an ER fluid, due to its ease of synthesis and conductivity control, good thermal and environmental stability (Jang *et al.*, 2001). Its rheological properties have been explored in terms of its yield stress (Jang *et al.*, 2001, Gozdalik *et al.*, 2000), as well as the oscillatory shear moduli and steady shear viscosity (Cho *et al.*, 2004, Hiamtup *et al.*, 2006), where the particle chains are continuously rupturing and reforming at or above some critical strain. However, to our knowledge, only a few studies of the creep behavior of PANI suspensions have been reported (Cho *et al.*, 2004, Hiamtup *et al.*, 2006) and none of these have investigated the effect of temperature on the creep response. In this paper, we explore the creep behavior of a polyaniline/silicone oil ER fluid, with particular attention to the effect of stress level, electric field strength, particle concentration, and operating temperature on the plastic deformation of the chain-like structure in the pre-yield regime.

6.3 Experimental

6.3.1 Materials

Aniline, C_6H_7N (AR grade, Merck) was vacuum-distilled and used as the monomer. Ammonium peroxydisulphate, $(NH_4)_2S_2O_8$ (AR grade, Merck) was used as the oxidant. 38 % Hydrochloric acid, HCl (AR grade, Labscan); 25 % solution of ammonia, NH_4OH (Ar grade, Merck) and methanol, CH_3OH (AR grade, Labscan) were used as received. The base fluid, a silicone oil (AR grade, Dow Corning) with density 0.96 g/cm^3 and kinematic viscosity of 100 cSt was vacuum-dried and stored in a desiccator prior to use.

6.3.2 Polymerization Procedure

PANI was synthesized via an oxidative coupling polymerization according to the method of Cao *et al.* (1989). After the course of polymerization, the precipitate was then dedoped by immersion in 3% NH_4OH in order to adjust its conductivity, before being vacuum dried and passed through a 38 μm sieve shaker to control the particle size and its distribution. The particle size was determined to be 23.5 ± 2.25 μm using a particle sizer. Scanning electron microscopy (SEM), Fourier transform infrared (FTIR) spectroscopy and thermogravimetric (TGA) analyses of the PANI material used in this study have been previously reported (Hiamtup *et al.*, 2006).

6.3.3 Preparation of ER Fluids

Prior to mixing in silicone oil, PANI powder was dried for 2 days at room temperature to remove moisture in a vacuum oven at room temperature. The particles were then dispersed in the silicone oil with an ultrasonicator for 30 minutes at 25 °C. The PANI suspensions were then prepared at volume fractions of 0.024, 0.048, and 0.092. The suspensions were stored in a dessiccator and redispersed by ultrasonification for a period of 10 minutes at 25 ^{0}C before each experiment.

6.3.4 Yiels Stress and Creep Measurements

The yield stress of the ER structures and also their creep and recovery behaviors were evaluated using a controlled-stress rheometer (Carrimed, CR50) with 4 cm diameter parallel plate geometry. The gap for the geometry used was 0.2 mm

for each measurement. Thus the ratio of gap width to mean particle size is ~ 8.5. A DC voltage was applied during the measurements using a high power supply (Bertan Associates Inc., Model 215) wherein the applied voltage could be precisely controlled. For the initial conditioning, the suspensions were subjected to a steady shear at 300 s^{-1} for 120s, after which the flow was stopped and the electric field applied for 10 minutes to obtain a steady-state fibrillar structure before each measurement was taken. In the yield stress experiment, a thixotropic loop test was first performed, in which the shear stress was slowly ramped up at a rate of 12 Pa/min, and the stress at which the material started to flow was recorded as the static yield stress. Subsequently, the stress was ramped down at the same rate, and the stress at which flow ceased designated as the dynamic yield stress. After the loop test, a series of creep compliance and recovery experiments were performed, such that a constant stress was instantaneously applied, maintained for 200 s, and then suddenly removed. The apparent equilibrium compliance J_e^{app} was measured at t = 200s, as the applied stress was sequentially increased to the yield point. J_e^{app} and the percent recoverable compliance were measured as a function of electric field strength, concentration, and temperature. After each creep test, the specimen was subjected to steady shear at 300 s^{-1} for 120s to erase prior history.

6.4 Results and Discussion

6.4.1 Thixotropic Loop Tests

Initially, thixotropic loop tests were performed at 298 K on three PANI suspensions in a controlled stress mode. The suspensions were prepared at volume fractions of 0.024, 0.048, and 0.092 in silicone oil as listed in Table 6.1. The dedoped (emeraldine base form) specimen of PANI used in our work has an electrical conductivity value of 2.93 x 10^{-9} S/cm. A PANI of low conductivity was chosen in order to enable us to investigate ER behavior at high electric field strength without current leakage in the system. Figure 6.1 shows the loop tests performed on a PANI suspension of 0.048 volume fraction at four applied electric field strengths. The static yield stress, σ_y(static) was determined as the applied stress immediately

prior to the onset of flow; the dynamic yield stress, σ_y(dynamic), was determined as the stress level on the downward part of the loop, at which flow ceased. The results are presented in Table 6.1. In the absence of an electric field, the particles are randomly dispersed in the dispersion, which exhibits a small yield stress (σ_y(static) ~ 0.2 Pa) followed by Newtonian flow, i.e. the dispersion shows Bingham fluid behavior (Figure 1a), with very little hysteresis. Upon application of an electric field of 1 kV/mm, the yield stress increases by an order of magnitude, reflecting the formation of the fibrillar ER structure, and there appears a substantial hysteresis in the loop test, i.e. a large difference between the values of σ_y(static) and σ_y(dynamic), which increases as the applied field is further increased. Consistent with results of prior controlled-stress thixotropic loop tests on ER fluids (Choi *et al.*, 1999), we find the dynamic yield stress is smaller than the static yield test, but, contrary to the earlier study, we do not observe a crossover from thixotropic behavior at low shear rates to anti-thixotropic behavior at high shear rates.

The temperature dependence of σ_y (static) and σ_y (dynamic) was explored for the PANI suspension of 0.092 vol fraction under an electric field strength of 2 kV/mm. The results are shown in Figure 6.2, and indicate that both σ_y(static) and σ_y (dynamic) increase with increasing temperature. Hao (Hao *et al.*, 2002) has discussed the forces which contribute to the ER effect, and the dimensionless groups which can be used to describe their relative importance. The Mason number indicates the ratio of hydrodynamic to electrostatic polarization forces, $Mn = 6\pi\eta \dot{\gamma}/\varepsilon_o\varepsilon_m(\beta E)^2$, where η_m is viscosity of the dispersing medium, $\dot{\gamma}$ is the shear rate, ε_o is permittivity of free space, $\beta = (\varepsilon_p-\varepsilon_f)/(\varepsilon_p+2\varepsilon_f)$, ε_m and ε_p are the static dielectric constants of dispersing medium and dispersed particles, and E is the applied electric field, whereas the Peclet number indicates the ratio of the hydrodynamic to thermal forces, $Pe = 6\pi\eta_m a^3 \dot{\gamma}/k_BT$, where a is the particle radius, k is the Boltzmann constant, T is temperature (K). The influence of temperature on yield stress may be viewed as deriving from the net effect of two contributions: one is the enhancement of Brownian thermal forces at high temperature which tends to weaken the ER effect, the other is the change in the electrostatic polarization force, which may either strengthen or weaken the ER effect. It follows that the ratio of

thermal to polarization forces scales as $Mn/Pe = k_BT/ \pi a^3 \varepsilon_o \varepsilon_m (\beta E)^2$. Evidently, in the case of these PANI suspensions, the results in Figure 6.2 suggest that the polarizability increases with temperature in the range 283 K -358 K to an extent that dominates over the contribution from Brownian motion. In contrast, experimental studies of the temperature dependence of the conductivity of PANI indicates that it exhibits a distinct maximum nearing the range T = 30 - 60 °C, depending on the sample thermal history (Mzenda *et al.*, 2002). Moreover, previous studies of the temperature dependence of the ER yield stress in PANI suspensions observe a weak maximum, coinciding with the observed maximum in PANI conductivity (Lee *et al.*, 1998, Xie *et al.*, 1996). However, we note that these studies have focused on the dynamic yield stress, measured by extrapolation to zero shear of the stress generated in a *controlled-shear rate* sweep. We conclude later that the enhanced strength we observe at higher temperatures, in σ_y(static) and σ_y(dynamic) from *controlled-stress* thixotropic loops, may originate in the strain-hardening effect discussed below.

6.4.2 Creep Tests: Effect of Applied Stress

The effects of stress level, particle concentration, and temperature on the creep compliance and recovery for the three PANI suspensions were investigated. Creep is the time-dependent increase in strain (γ) of a viscoelastic material under sustained stress (σ) in which some of the time-dependent deformation may be recoverable with time after the removal of stress (Klingenberg, 1993). Creep and recovery curves for a typical nonlinear viscoelastic material are illustrated schematically in Fig. 6.3. The time dependence of strain can be expressed as follows;

$$\gamma(t) = \gamma_s + \gamma_d(t) + \gamma_v(t) \qquad (1)$$

where γ_s is the instantaneous strain, $\gamma_d(t)$ a retarded elastic strain, and $\gamma_v(t)$ the viscous flow or an irreversible component of strain. For nonlinear viscoelastic materials, the instantaneous strain γ_s may consist of an elastic component and a plastic component γ_p, the latter cannot be recovered after unloading. For magnetorheological (Klingenberg, 1993) and electrorheological (Mcleish *et al.*, 1991) fluids, it has been established that increase of applied stress, relative to constant field strength, causes an evolution from a linear elastic, to linear viscoelastic response, with the above three components of instantaneous elastic strain, retarded elastic strain and viscous

strain, then to a nonlinear viscoelastic response, where the retarded elastic and viscous strains monotonically decrease and a plastic contribution to the instantaneous strain grows, followed by a viscoplastic solid behavior, with fully plastic instantaneous strain, and finally a transition from plastic solid to viscous flow when the yield stress is exceeded.

The creep compliance, J(t) is defined as the time-dependent strain $\gamma(t)$ divided by the applied stress, σ:

$$J(t) = \gamma(t) / \sigma \qquad (2)$$

J(t) is a material function which describes the ease of deformation of the ER fluid under the specified applied stress (Chotpattananont, 2004). We determined J_e^{app}, the apparent equilibrium creep compliance, measured after a stress below the yield stress has been applied for a duration of 200s, as well as J_r, the steady state recoverable compliance, at 300s after the stress is removed.

Fig. 6.4 shows the creep and recovery curves for a 4.8 vol % PANI suspension under an electric field strength of 4 kV/mm with applied shear stresses of 100, 120, 150, 155, 180, and 200 Pa at 298 K. From Fig. 6.4a, at 100 Pa, we are already in the nonlinear viscoelastic regime, since the instantaneous strain, γ_s, is larger than the instantaneous elastic recovery, γ_e, indicating a substantial plastic contribution, γ_p, to the instantaneous strain, (Klingenberg, 1993, Mcleish et al., 1991), which grows as the stress is increased to σ = 150 Pa. It is interpreted that the elastic response comes from the stretching of particle strings within thick columns, which span the fluid between the electrodes, and which is recoverable after stress removal, while the plastic response derives from deformation of unattached strings, and strings attached at one electrode only, as well as structural rearrangements within doubly-attached strings, all of which dissipate stress, and are non-recoverable (Klingenberg, 1993, Mcleish et al., 1991, Parthasarathy and Klingenberg, 1996, Lau et al., 2003). In Figure 6.4b we find that, on increasing the applied stress from 150Pa to 155 Pa, there is a surprisingly large increase in the plastic strain which the system can support prior to yield, (from γ = 0.89 to γ = 65). This corresponds to an increase in the rotation of the plate from 0.5° to 37°. As the stress is increased further to 200 Pa, the plate is able to rotate 2.6 times in 12 seconds (strain of 1636) before coming

to a halt. Note, however, that the quoted strain is the edge strain, and in fact, in parallel plate geometry, the particle columns are subjected to a wide range of deformations from very small $\gamma \sim 0$ near the center to $\gamma = 1636$ at the edge. It seems clear however that towards the edge, particle columns must experience increasing amounts of stretching, slippage, structural rearrangement, and/or break-up and reformation. As the stress is increased further beyond 200 Pa, the sample yields and flows. In Figure 6.2, we plot the yield stress values $\sigma_{y(creep)}$, determined from the onset of flow in the creep tests. Values of $\sigma_{y(creep)}$, listed in Table 6.1 and plotted in Figure 6.2, are the mean of two or three repeated measurements. It is noteworthy that $\sigma_{y(creep)}$ is substantially smaller than $\sigma_{y(static)}$, particularly at lower temperatures. We attribute this difference to the fact that the $\sigma_{y(static)}$ values are determined by slowly ramping up the stress, whereas $\sigma_{y(creep)}$ involves instantaneous application of stress. The former treatment allows more time for implementation of the strain-hardening process, which is discussed later. Creep behavior of PANI suspensions has been reported previously by Gow and Zukoski (Gow and Zukoski, 1990), who primarily focused on the scaling of yield stress with field strength. From Table 6.1, we deduce $\sigma_{y(creep)} \sim E^{1.85}$, which seems consistent with scaling exponents in the range 1.56-2.25, as determined by Gow and Zukowski (Gow and Zukoski, 1990). Numerically comparable scaling exponents were determined from Table 1 for $\sigma_{y(static)}$ and $\sigma_{y(dynamic)}$.

In Fig. 6.5, we show the % recoverable strain plotted against the total strain supported by the sample in the pre-yield regime, for suspensions of different particle concentrations and at various applied field strengths. The % recovery is defined by the following equation;

$$\%\text{recovery} = \frac{(\gamma_i - \gamma_f)}{\gamma_i} \times 100 \qquad (3)$$

where γ_i is the acquired total strain before stress removal and γ_f is the residual strain after stress removal. The % recovery decreases monotonically with increasing total strain and becomes zero at the onset of the plastic solid regime. Moreover, it is noted that the recoverable strain disappears when the total strain is higher than a critical value in the range 0.4-0.5, independent of particle concentration and electric field

strength. This result appears to be reasonably consistent with literature values, 0.3-0.4, as reported by Otsubo and Edamura, 1994. In summary, the results in Figure 6.5 show the evolution from viscoelastic to viscoplastic deformation (0% recoverable strain) as the total strain on the sample increases beyond 0.4-0.5, and illustrate that the creep transition to large strains ($\gamma >> 1$) falls in the pre-yield viscoplastic response regime.

Based on such creep experiments, as illustrated in Figure 6.6, we consistently find a pre-yield transition to an apparently more ductile state, manifested as a discrete increase in the apparent equilibrium compliance sustained by the sample, at a stress value which we have designated the critical stress, σ_c. Fig. 6.6, shows the dependence on applied stress, σ, of the apparent equilibrium compliance, J_e^{app} of the PANI suspensions for various particle concentrations and electric field strengths at 25 °C, plotted in the form J_e versus σ. As expected, the results show that increase of particle concentration and electric field strength enhances the creep resistance of EB/Silicone oil suspension. Increase in electric field strength induces a higher dipole moment causing the particle chains to coalesce and form thicker chains (Shi *et al.*, 2006). Likewise, a higher particle concentration results in a denser fibrillar structure (Cho *et al.*, 2004) and hence a higher rigidity. Also evident in Figure 6.6, however, is the fact that we observe an abrupt increase in J_e as the magnitude of applied stress exceeds the critical stress, σ_c. As seen in Figure 6.6, PANI samples of volume fractions 2.4 vol % and 4.8 vol % exhibit the transition at T = 298 K. The sample having 9.2 vol % PANI appears to show the transition, but was not able to support such large apparent strains as the samples of lower concentration at 298 K. The abrupt shift to higher J_e indicates that, above σ_c, the suspension begins to yield, but that the yielding process arrests itself, presumably because the sample develops an enhanced ability to sustain the load or deformation, which implies a process of strain-hardening of the fibrillar structure. As support for this idea, we note that a strain-hardening effect has been recently reported in a model ER fluid, consisting of silica particles dispersed in a silicone oil, manifested as an enhancement of the yield stress, when the fluid was subjected, using parallel plate geometry, to

repeated creep-recovery cycles in the presence of an applied field (Lau *et al.*, 2003, Shi *et al.*, 2006).

The temperature dependence of J_e^{app} was examined for 9.2 vol% PANI, and is shown in Figure 6.7. Here we find that, on increasing temperature up to 358 K, the J_e curves shift to the right, which implies that the creep resistance increases as the operating temperature increases, an observation which is consistent with the temperature dependence of yield stress shown in Fig. 6.2 Moreover, it can be seen that the value of σ_c, at which the transition to an apparently more compliant structure occurs, increases with increase in temperature. In Figure 6.6b, we replot the J_e^{app} data for 0.92 vol% PANI at $T \geq 313$ K in the form ln J_e^{app} versus linear stress, to illustrate that, above and below the transition, the stress dependence of J_e^{app} appears to exhibit an exponential dependence on the applied stress, σ. Intuitively, if, as noted earlier, the temperature dependence of the yield stress is determined by the ratio of the polarization stress to the Brownian stress, one might anticipate that the equilibrium compliance is inversely related to this ratio. This suggests the following relationship:

$$J_e^{app} = J_{e,0}^{app} \exp\left(\frac{\alpha \sigma k_B T}{\pi a^2 \varepsilon_0 \varepsilon_m (\beta E)^2} \right) \qquad (5)$$

where $J_{e,0}^{app}$ is the hypothetical creep at infinitestimally small σ. For $\sigma < \sigma_c$, this corresponds to the value of J_e^{app} at the limit of linear viscoelasticity. In equation (5), the prefactor α is a scaling parameter, presumed constant for a particular fibrillar ER structure

The slopes of the plots of ln J_e^{app} versus σ in fig. 6.6b, measured above and below σ_c, are tabulated in Table 6.1. Interestingly, Table 6.1 shows that, for the sample having PANI volume fraction $\phi = 0.048$ at 298 °K, the slopes decrease proportionally to the square of the electric field, which is consistent with equation (5). However, for the PANI sample having $\phi = 0.092$, Figure 6b and Table 6.1 indicates the slope decreases with increasing temperature, which appears to conflict with equation (5), since the conductivity decreases in this temperature range (Li *et al.*, 2002). As for the anomalous temperature dependence of the yield stress, we infer below that this phenomenon arises because of the strain-hardening phenomenon that

occurs in controlled-strain parallel plate geometry, which effectively leads to an increase in the prefactor α.

The values of σ_c are also listed in Table 6.1. Comparing σ_c versus $\sigma_{y(static)}$, $\sigma_{y(dynamic)}$, and $\sigma_{y(creep)}$, we find that σ_c lies numerically near or just below the dynamic yield stress. These observations suggest that during the creep test in parallel plate geometry, when the applied strain exceeds σ_c, a strain hardening process occurs in the fibrillar ER structure. In other words, the sample starts to yield at σ_c but the strengthening process arrests creep until the applied strain exceeds $\sigma_{y(creep)}$ of the hardened fibrillar structure.

As a test of this hypothesis, the yield stress of pre-strained ER structures was evaluated for a 9.2 vol% PANI suspension at 328 K, by performing thixotropic loop tests immediately after creep experiments performed at stresses above the σ_c transition point. Thus, in Fig. 6.8, we show a series of creep experiments performed on this particular 9.2 vol% PANI suspension, under an applied field of 1 kV/mm, with shear compliance plotted in log scale versus linear time, so that we can exhibit the creep response through the yield point. As the stress is increased up to 112 Pa, the creep response evolves through viscoelastic to plastic solid behavior. On increasing stress from 112 Pa to 115 Pa, there is again a discrete transition in instantaneous compliance, from $J = 0.0181\ Pa^{-1}$ ($\gamma = 2.02$) to $J = 0.373\ Pa^{-1}$ ($\gamma = 42.8$). At $\sigma = 150$ Pa, we see the onset of viscous flow, since the strain does not reach an equilibrium value after 200 sec. From this we estimate the yield stress from the creep experiments, $\sigma_{y(creep)} = 140$ Pa.

Figure 6.9 compares a thixotropic loop performed on the unstrained 0.092 volume percent PANI sample studied in Fig. 6.8, with loops performed immediately after creep experiments in which the sample was subjected to applied stresses of, respectively 110, 150 and 170 Pa, in each case maintained for 200 sec. Comparing Fig. 6.9(a) versus Fig. 6.8, we see that $\sigma_{y(static)} = 190.1$ Pa, substantially larger than $\sigma_{y(creep)} = 140$ Pa measured on the sample. From Figs 6.9(b), 6.9(c), and 6.9(d), it is clear that the static yield stress of the pre-strained suspensions is substantially higher than that of the unstrained sample. The dynamic yield stress, measured from the intercept on the downward part of the loop, remains unchanged at

150 Pa. This suggests that the strain-hardening process contributes to the hysteresis observed in the thixotropic loop. In Figure 6.10, we plot the variation of static yield stress measured on prestrained samples as a function of the pre-straining stress. Evidently, the magnitude of strain-hardening increases with the applied stress up to 140 Pa, then decreases. This indicates that the strain hardening becomes less effective with the onset of flow in the suspension, since flow is observed when σ = 150 Pa and 170 Pa (Fig. 6.8). As noted by Tam *et al.* (Lau *et al.*, 2003, Shi *et al.*, 2006), on application of the electric field the columnar structures formed may be viewed as metastable structures, with many defects. The application of shear strain may remove such defects via slippage and restructuring, leading to mechanically stronger columns. In addition, analysis of the crystalline organization of the columnar structures induced by the electric field (Tao and Sun, 1991; Davis, 1992 and Dassanayake *et al*, 2000), suggests that deformation may transform the crystal structure from some lower energy structure to a different, stronger one; e.g. face-centered or body-centered tetragonal may transform to a hexagonal close-packed lattice. Finally, it has been suggested that, after deformation, the ER structure may consist not only chains of particle columns spanning the electrode gap along the field direction (primary chains), but may also have secondary structures, short tilted chains which interconnect the primary chains, and which strengthen the ER structure (Pan and Mckinley, 1997). In the present study, we note that the PANI particles have irregular shapes, and a wide size distribution, and therefore are not expected to form an ordered lattice-like structure. However, it appears that a strengthening process can still take place, presumably via rearrangement of the particles within the strained fibrils to form a more dense interparticle organization.

It remains to attempt a more detailed explanation of the apparent ductility transition in terms of the strain-hardening phenomenon reported by Tam and coworkers (Lau *et al.*, 2003, Shi *et al.*, 2006). These studies observed shear-hardening when the ER fluid was subjected to repeated creep-recovery cycles using applied stress values ranging up to, and slightly larger than, the yield stress. In our experiments, we observe the discrete increase in apparent compliance when the applied stress approaches the yield point $\sigma_{y(creep)}$ in parallel plate geometry. The ER fluid near the center does not experience a large strain, and so near the center the

particle strings may be unbroken, even at relatively large edge strains. It follows that there would be a boundary between unbroken and broken strings at some radius. At the boundary radius there is a dynamic equilibrium mixture of broken and unbroken strings, the relative numbers of each being determined by the average modulus (stress/strain) of the unbroken strings. Following Tam et al. (Lau *et al.*, 2003, Shi *et al.*, 2006), we assume the unbroken strings experience strain hardening on stretching, and therefore the average local modulus increases with time. Since there is a dynamic equilibrium in which strings are breaking and reforming, it therefore seems possible that the fraction of broken strings at that radius decreases with time. This provides a possible mechanism that the boundary between broken and unbroken strings moves toward the edge of the parallel plates, until all the strings are stronger and unbroken and the plate comes to a halt. Consequently, when a loop test is performed, after this process is complete, and the sample is annealed under these conditions, the static yield stress increases over that measured in the unstressed sample. Such a phenomenon, the apparent ductile transition, may therefore be unique to parallel plate and therefore not present in Couette, or cone and plate.

Finally, we note two consequences of the strain-hardening effect. First, it follows that strain hardening is a prime contributing factor to the hysteresis manifested in controlled-strain thixotropic loop tests (Figure 6.1). Second, we infer that the strain-hardening process is the reason that $\sigma_{y(static)}$, $\sigma_{y(dynamic)}$, and $\sigma_{y(creep)}$ data obtained in our controlled stress creep experiments do not correlate to the maximum observed in the conductivity of PANI (Figure 6.2). Presumably, a decrease in polarization forces with increased temperature may facilitate the particle rearrangements necessary to form the hardened structure.

6.5 Conclusions

Thixotropic loop experiments performed on PANI/silicone oil ER fluids show a pronounced hysteresis. The magnitude of the hysteresis may be gauged from the difference between the values of the static yield stress, $\sigma_{y(static)}$, measured from the onset of flow in the upward segment of the loop, and the dynamic yield stress,

$\sigma_{y(dynamic)}$, measured from the cessation of flow on the downward segment. The magnitude of the hysteresis increases with increase of electric field strength and particle concentration, and decreases with increase of temperature. With increasing applied stress, the creep response of the PANI/silicone oil suspensions, under a constant electric field shows an evolution from a nonlinear viscoelastic response, at low applied stress to a viscoplastic solid behavior and finally to viscous flow. The yield stress measured from creep experiments, $\sigma_{y(creep)}$, typically falls between the values of $\sigma_{y(static)}$ and $\sigma_{y(dynamic)}$, but closer to $\sigma_{y(dynamic)}$. The onset of viscoplastic solid response in the creep curve appears to occur when the instantaneous strain reaches a nonrecoverable critical value of the order 0.4-0.5. At strains above this value, an unusual phenomenon is observed in the form of a discrete increase in the apparent equilibrium compliance. Thixotropic loop experiments performed after strain annealing suggest this phenomenon is due to strain hardening of the ER fibrillar structures, presumably due to particle rearrangements to form a denser, more defect-free configuration. We infer that the strain-hardening process contributes to the hysteresis observed in the thixotropic loop test and the enhanced yield strength at high temperatures.

6.6 Acknowledgements

The authors would like to acknowledge the financial support provided by The Thailand Research Fund (TRF) RGJ grant no. PHD/0234/2544 and BRG, Conductive & Electroactive Polymers Research Unit and KFAS of Chulalongkorn University, and the Petroleum Petrochemical and Advanced Materials Consortium, and Royal Thai Government (Budget of Fiscal Year 2550). AMJ also wishes to acknowledge financial support from the National Science Foundation, Polymers Program, under grant no. DMR 0513010

6.4 References

Akella, P.N. and Cutkosky, M.R. (1995). Contact transition control with semiactive soft fingertips. IEEE Trans. Robotics Automat., 11(6), 859-867.

Bohon, K. And Krause, S. (1998). An electrorheological fluid and siloxane gel based electromechanical actuator: working toward an artificial muscle. J. Polym. Sci. B., 36, 1091-1094.

Cao,Y., Andreatta, A., Heeger, A.J., and Smith,P. (1989). Influence of chemical polymerization conditions on the properties of polyaniline. Polymer, 30, 2305-2311.

Cho, M.S., Lee, J.H., Choi, H.J., Ahn, K.H., and Lee, S.J. (2004). Linear viscoelasticity of semiconducting polyaniline based electrorheological suspensions. J. Mater. Sci., 39, 1377-1382.

Choi, H. J., Cho, M. S., Jhon, M. S. (1999). Int. J. Mod. Phys. B, 13, 1901.

Choi, S.B., Choi, Y.T., Chang, E.G., Han, S.J., and Kim, C.S. (1998). Control characteristics of a continuously variable ER damper. Mechatronics, 8, 143-161.

Chotpattananont, D., Sirivat, A., and Jamieson, A.M. (2003). Electrorheological properties of perchloric acid-doped polythiophene suspensions. Colloid Polym. Sci., 282, 357-365.

Chotpattananont, D., Sirivat, A., and Jamieson, A.M. (2006). Creep and recovery behaviors of polythiophene-based electrorheological fluid. Polymer 47, 3568-3575.

Dassanayake, U., Fraden, S., and Blaaderen, A.V. (2000). Structure of electrorheological fluids. J. Chem. Phys., 12(8), 3851-3858.

Davis, L.C. (1992). Ground state of an electrorheological fluid. Phys. Rev. A46(2), R719-R721.

Gow, C. J. and Zukoski, C. F. (1990). The electrorheological properties of polyaniline suspensions. J. Coll. Interf. Sci., 136, 175-188.

Gozdalik, A., Wycislik,H., and Plocharski, J. (2000). Electrorheological effect in suspensions of polyaniline. Synt. Met., 109, 147-150.

Hao, T. (2002). Adv. Coll. Interface Sci., 97, 1.

Hiamtup, P., Sirivat, A., and Jamieson, A.M. (2006). Electrorheological properties of polyaniline suspensions: field-induced liquid to solid transition and residual gel structure. J. Colloid. Interf. Sci., 295, 270-278

Jang, W.H., Kim, J.W., Choi, H.J., and Jhon, M.S. (2001). Synthesis and electrotheology of camphorsulfonic acid doped polyaniline suspensions. Colloid. Polym. Sci., 279, 823-827.

Kamath, G.M. and Wereley, N.M. (1997). A nonlinear visoelastic-plastic model for electrorheological fluids. Smart Mater. Struct., 6, 351-359.

Klingenberg, D.J. (1993). Simulation of the dynamic oscillatory response of electrorheological suspensions: demonstration of relaxation mechanism. J. Rheol., 37, 199-214.

Lau, K. C., Shi, L., Tam, W. Y., Sheng, P. (2003) Shear-enhanced yield stress in electrorheological fluis. Phys. Rev., E 67, 052502.

Lee, H.-J., Chin, B.D, Yang, S.-M., Park, O.O. (1998) Surfactant effect on the stability and electrorheological properties of polyamiline particle suspension. J. Colloid. Interface. Sci. 206, 424-438.

Li, W.H., Du, H., Chen, G. and Yeo, S.H. (2002). Experimental investigation of creep and recovery behaviors of magnetorhelogical fluids. Mater. Sci. Engr., A333, 368-376.

Lu, J. and Zhao, X. P. (2002). Int. J. Mod. Phys. B 16, 2521-2527.

Mcleish, T.C.B., Jordan, T., Shaw,M.T. (1991). Viscoelastic response of electrorheological fluids I. Frequency dependence. J. Rheol., 35(3), 427-448.

Mzenda, V.M., Goodman,S.A., Auret, F.D., and Prinsloo, L.C. (2002). Characterization of electrical charge transfer in conductive polyaniline over the temperature range $300 < T(K) < 450$. Synt. Met., 127, 279-283.

Otsubo,Y. and Edamura, K. (1994). Creep behavior of electrorheological fluids. J. Rheol., 38(6), 1721-1733.

Pan, X.D. and McKinley, G.H. (1997). Structural limitation to the material strength of electrorheological fluids. Appl. Phys. Lett., 71(3), 333-335.

Papadopoulos, C.A. (1998). Breaks and cluthes using ER fluids. Mechatronics, 8 719-726.

Parthasarathy, M. and Klingenberg, D. J. (1996). Electrorheology: mechanisms and models. Mater. Sci. Eng., R17, 57-103.

Shi, L., Tam, W. Y., Huang, X. X., Sheng, P. (2006) Static shear modulus of electrorheological fluids. Phys. Rev., E, 73, 051501.

Tao, R. and Sun, J.M. (1991). Three-dimensional structure of induced electrorheological solid. Phys. Rev. Lett., 67, 398-438.

Winslow, W.M. (1949). Induced fibrilation of suspensions. J. Appl Phys., 20, 1137-1140.

Xie, H.-Q. and Guan, J.-G. (1996). Die Angew. Makromol. Chem. 235, 21.

Yanju, L., Hejun, D., and Dianfu, W. (2001). ER fluid based on inorganic/polymer blend particles and its adaptive viscoelastic properties. Colloid. Surf., A189, 203-210.

Table 6.1 Characteristic parameters describing yield behavior of PANI/Silicone oil suspensions as a function of particle concentration, temperature and electric field strengths

Sample	Φ	E (kV)	Temp (K)	σ_y (static) (Pa)	σ_y (dynamic) (Pa)	σ_y (creep) (Pa)	σ_c (critical (Pa)
048-1kV	0.048	1	298	27.7±3.0	15.9±2.1	15.5	15.3
024-2kV	0.024	2	298	39.4±2.8	25.8±0.7	29.5	28.2
048-2kV	0.048	2	298	93.7±7.3	73.4±22.3	55	47
048-4kV	0.048	4	298	229.4±5.7	170.3±8.6	210	150
092-2kV	0.092	2	298	116.7±7.5	87.0±0.4	92	N/A
092-2kV	0.092	2	283	102.9±13.2	69.1±0.3	80	N/A
092-2kV	0.092	2	313	133.7±6.6	108.3±0	111	102
092-2kV	0.092	2	328	153.3±28.9	126.5±19.4	135	112
092-2kV	0.092	2	343	157.8±3.1	152.4±1.5	160	127
092-2kV	0.092	2	358	188.7±8.5	165.8±5.1	190	140

Slope* is the slope of ln J_e^{app} vs. T in Figure 6b

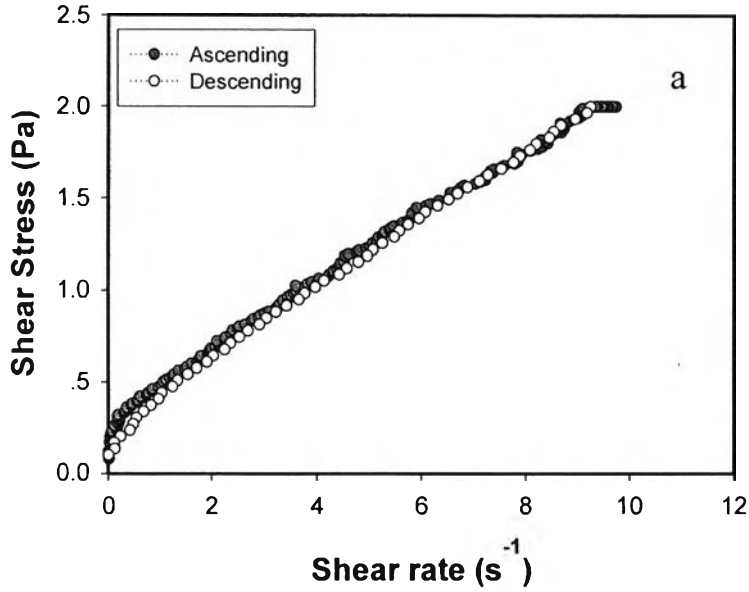
Ascending
Descending
a
Shear Stress (Pa)
2.5
2.0
1.5
1.0
.5
0.0
0
2
4
6
8
10
12
Shear rate (s-1)

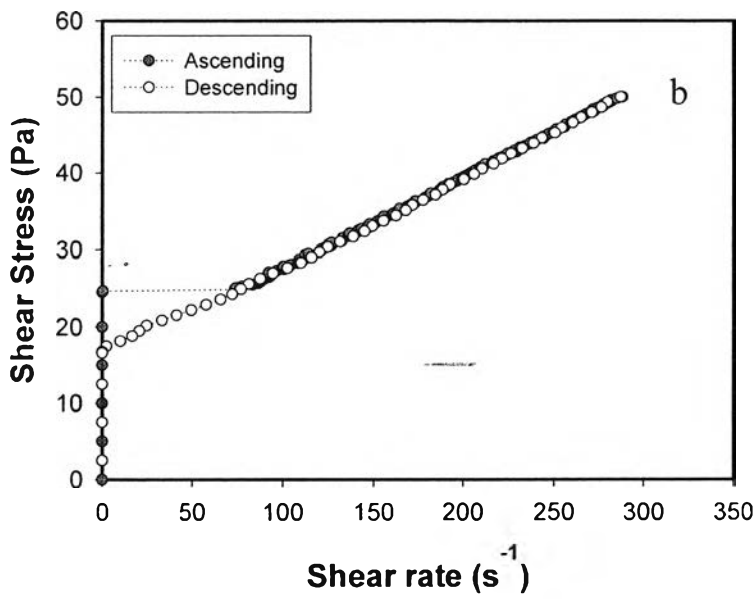
Ascending
Descending
b
Shear Stress (Pa)
60
50
40
30
20
10
0
0
50
100
150
200
250
300
350
Shear rate (s-1)

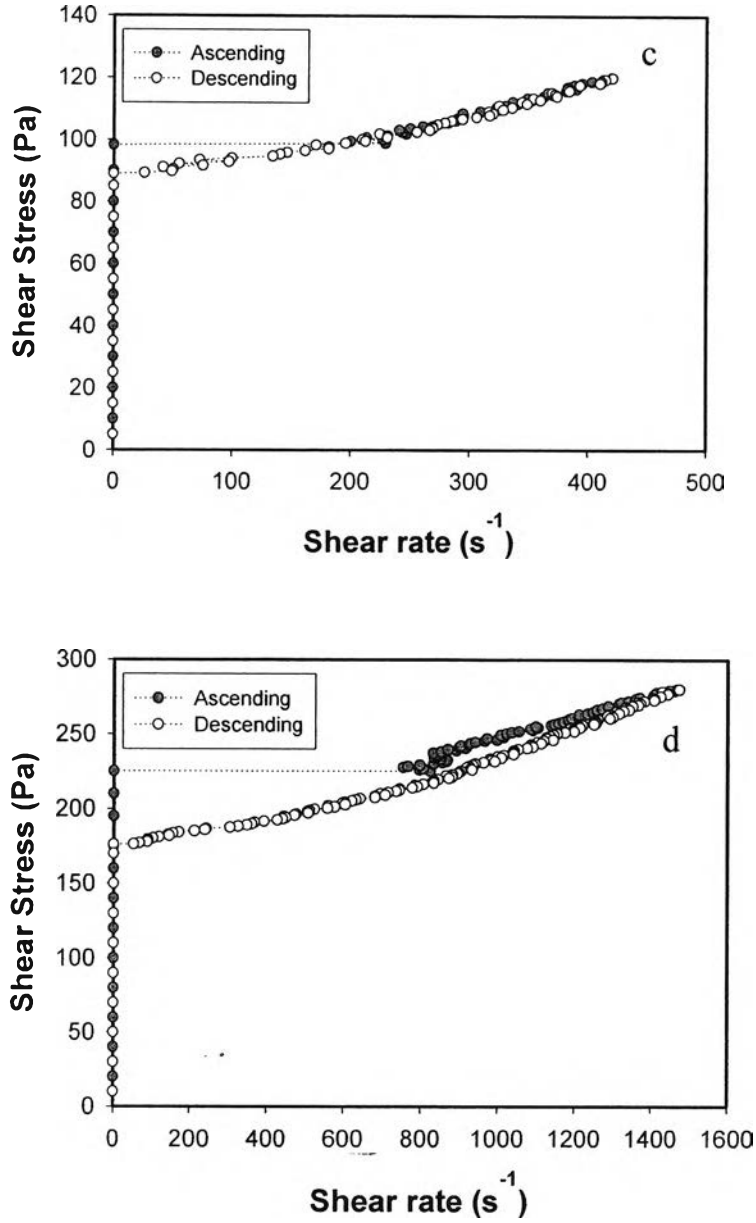

Figure 6.1 Thixotropic loop tests performed on a dispersion of 0.048 volume fraction PANI in silicone oil at three electric field strengths: (a) 0 kV/mm, (b) 1 kV/mm, (c) 2 kV/mm, and (d) 4 kV/mm.

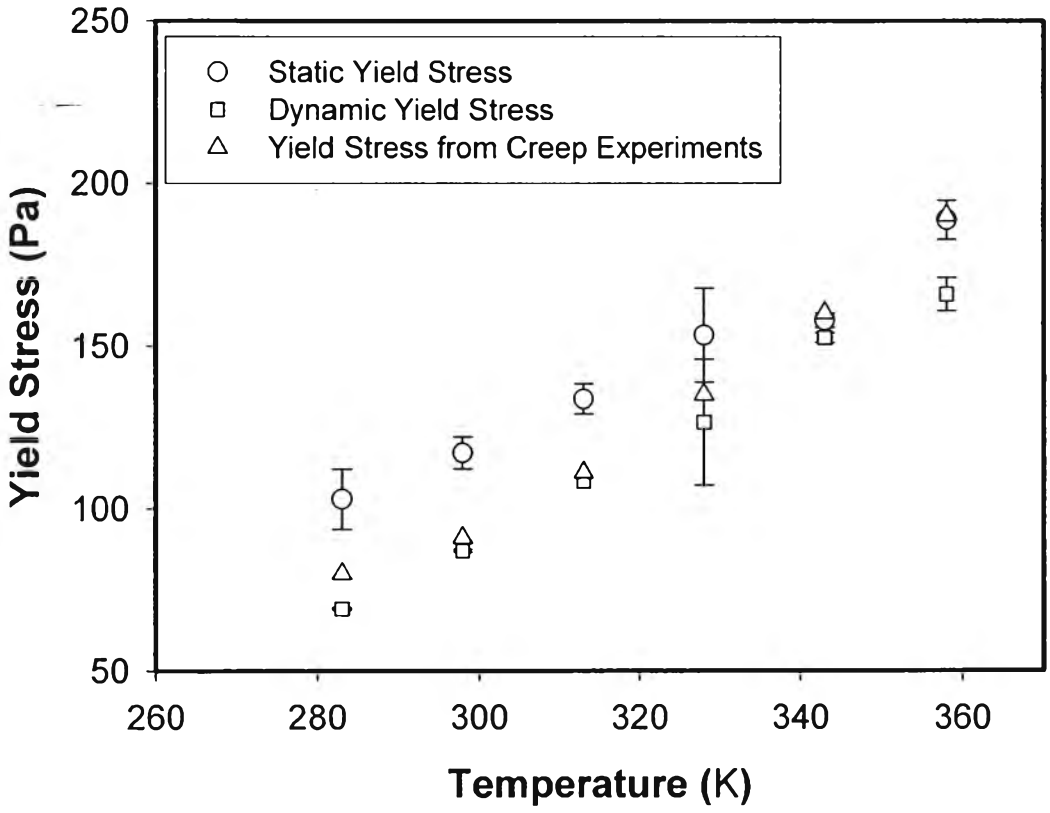

Figure 6.2 The dependence of yield stress on temperature of PANI/Silicone oil suspension, vol% = 9.2 at E = 2 kV/mm at various temperatures.

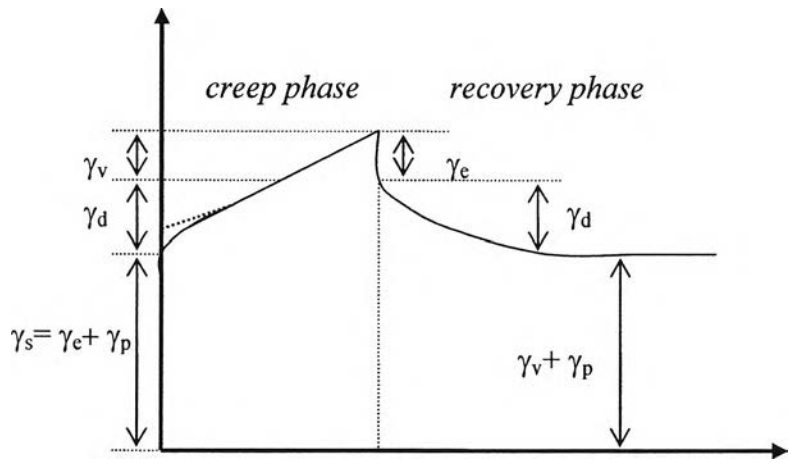

Figure 6.3 Schematic illustration of the creep and recovery behavior of a nonlinear viscoelastic liquid.

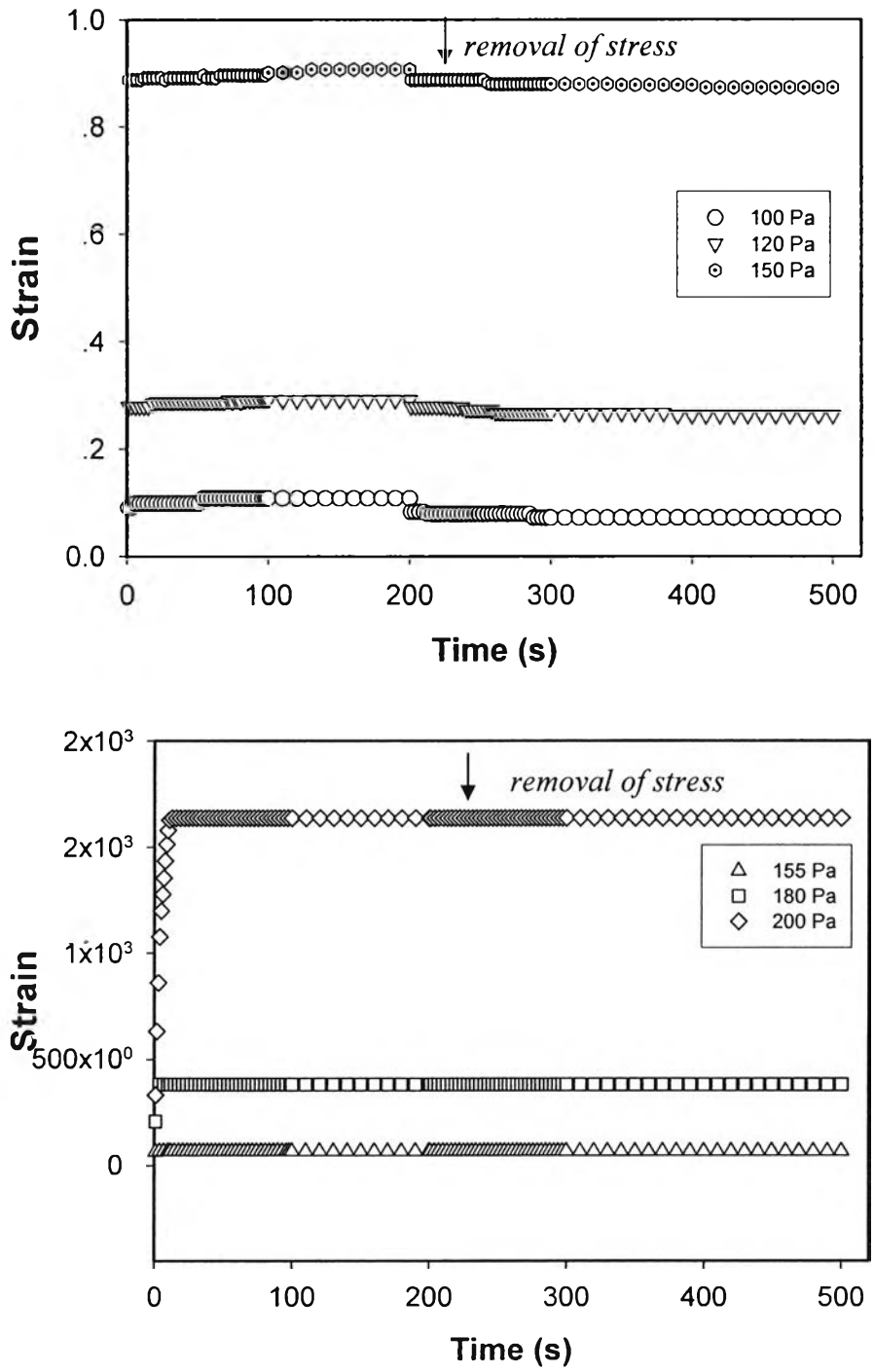

Figure 6.4 Creep and recovery curve of PANI /Silicone oil suspension, vol% = 4.8 under an electric field strength of 2 kV/mm at 298 K: (a) with applied stresses of 100 Pa, 120 Pa and 150 Pa; (b) with applied stresses of 155 Pa, 180 Pa and 200 Pa

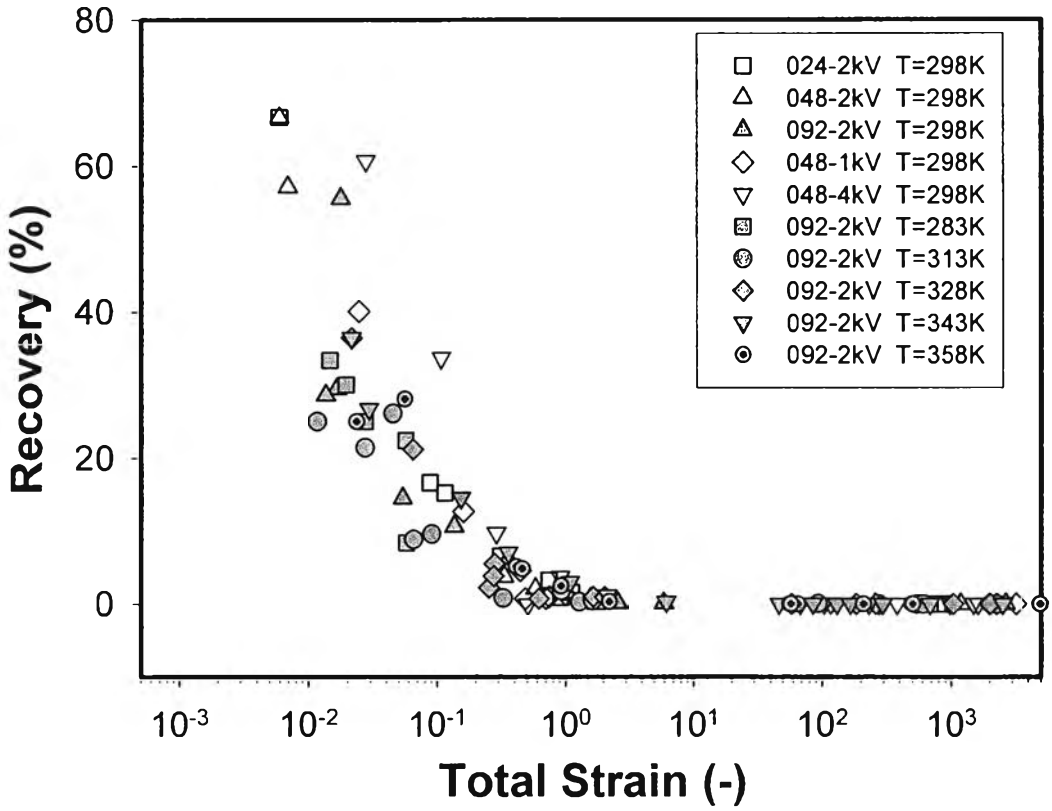

Figure 6.5 Percentage of the recoverable strain is plotted versus the total strain sustained by the PANI suspensions at various electric field strengths, concentrations and temperatures.

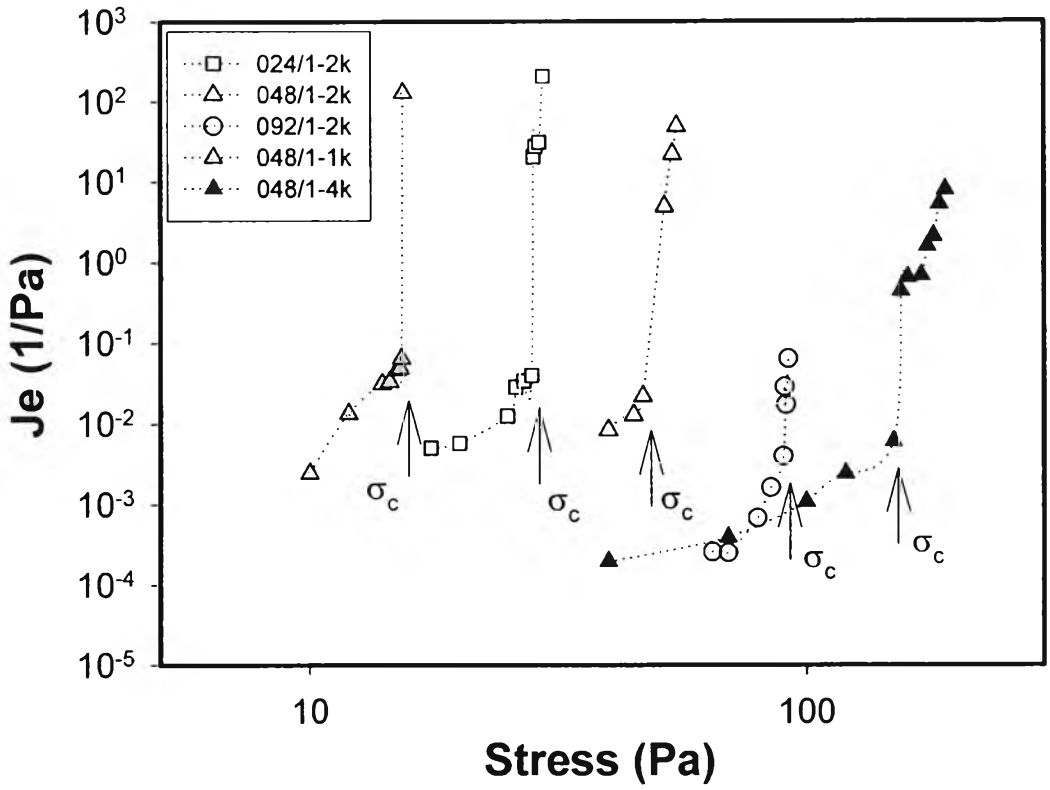

Figure 6.6 Creep compliance parameter J_e of PANI/Silicone oil suspension at various particle concentrations and various electric field strengths, where oil viscosity was fixed at 100 cSt, measured at T = 298 K: (□) vol% = 2.4 at E = 2 kV/mm; (Δ) vol% = 4.8 at E = 2 kV/mm; (○) vol% = 9.2 at E = 2 kV/mm; (△) vol% = 4.8 at E = 1 kV/mm; (▲) vol% = 4.8 at E = 4 kV/mm.

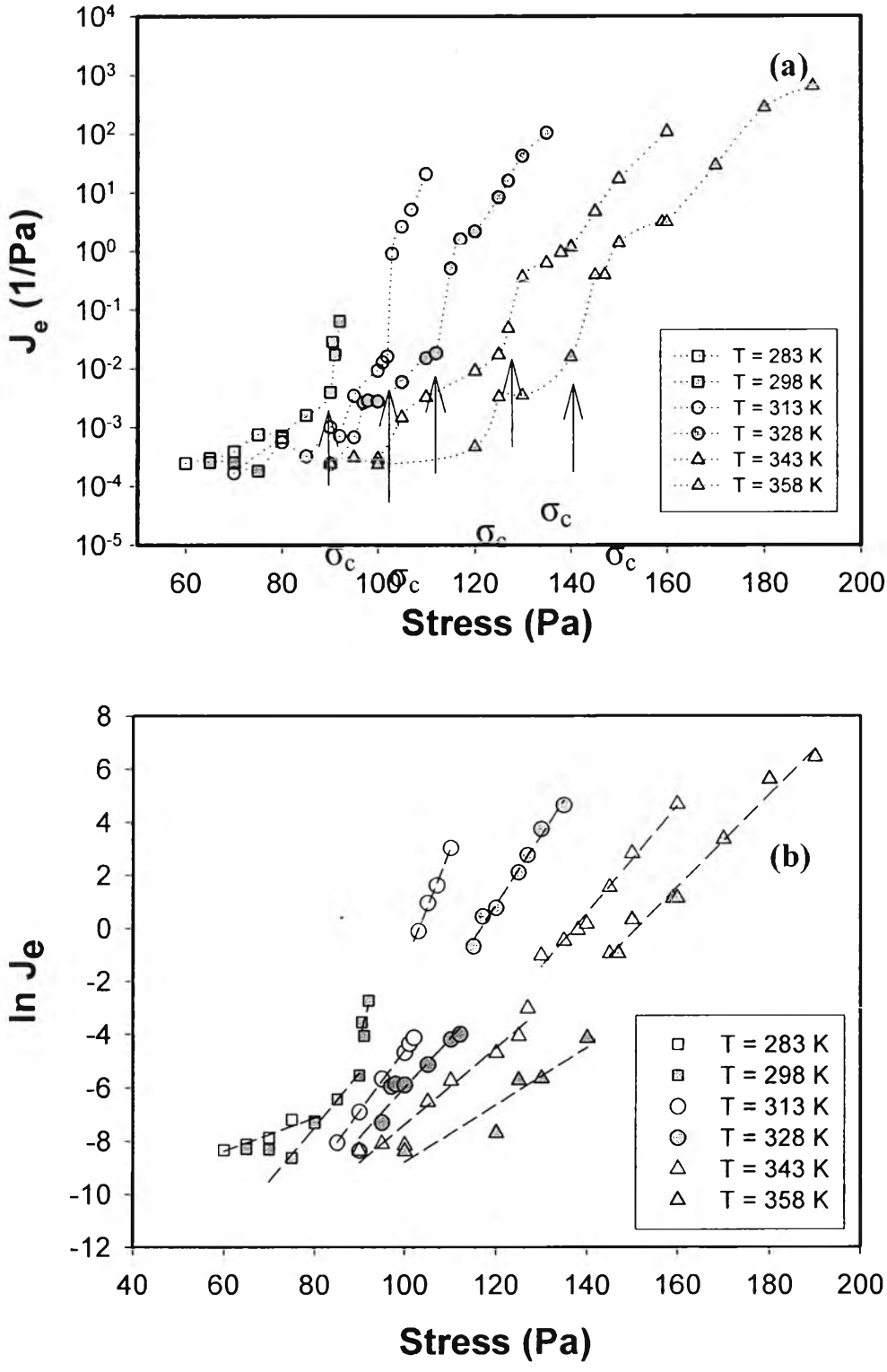

Figure 6.7 (a) Dependence of creep compliance on applied stress for 9.2 vol% PANI at various temperatures; (b) data in Fig. 6(a) replotted in the form ln J_e^{app} versus applied stress.

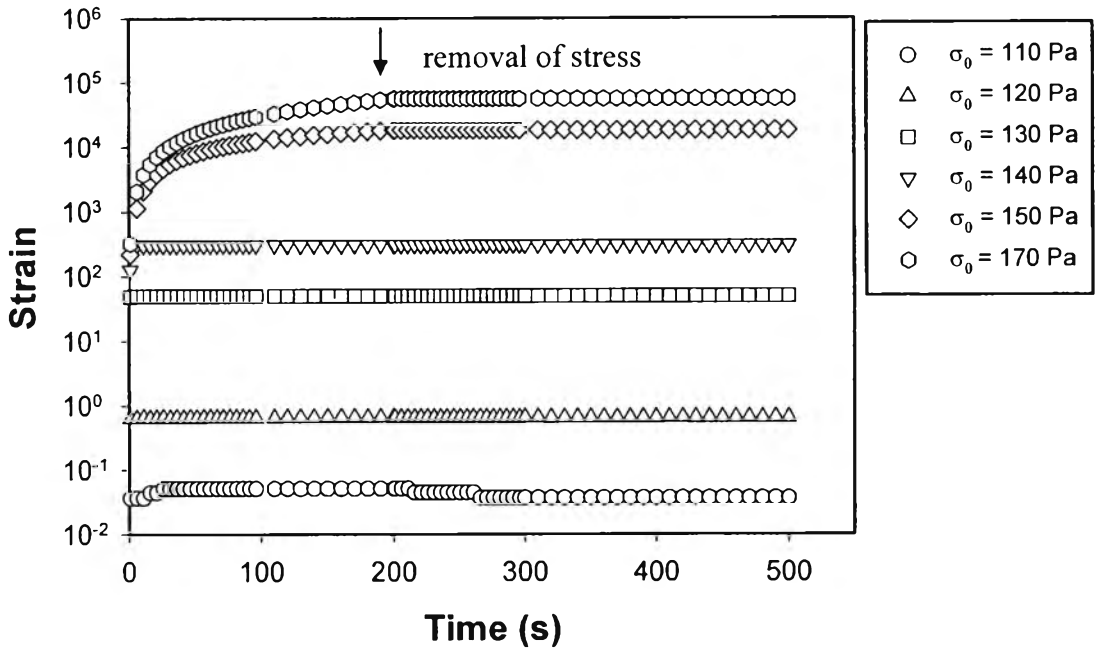

Figure 6.8 Creep and recovery of PANI /Silicone oil suspension, vol% = 9.2 under the electric field strength of 2 kV/mm at various applied stress values, T = 328K.

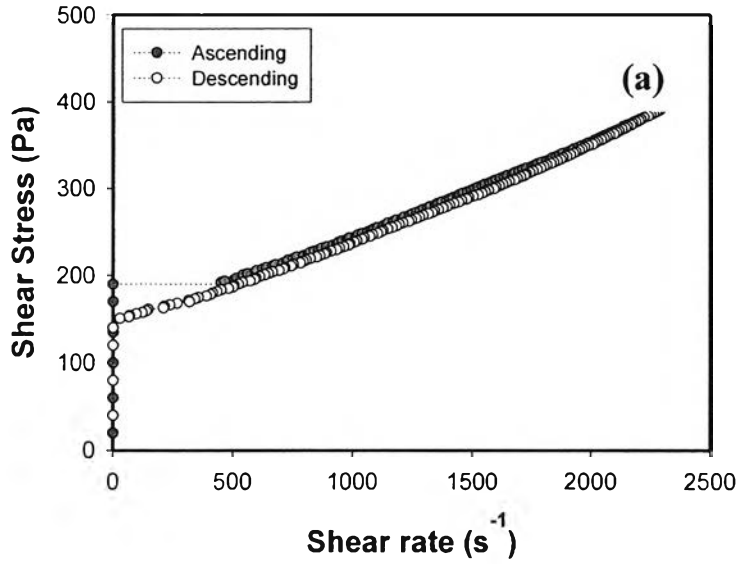
Ascending
Descending
(a)
Shear Stress (Pa)
Shear rate (s-1)
0
100
200
300
400
500
0
500
1000
1500
2000
2500

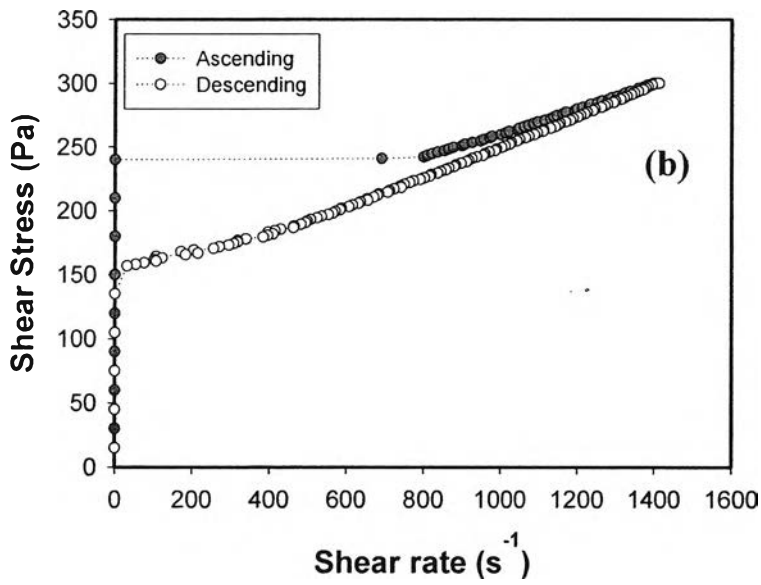
Ascending
Descending
(b)
Shear Stress (Pa)
Shear rate (s-1)
0
50
100
150
200
250
300
350
0
200
400
600
800
1000
1200
1400
1600

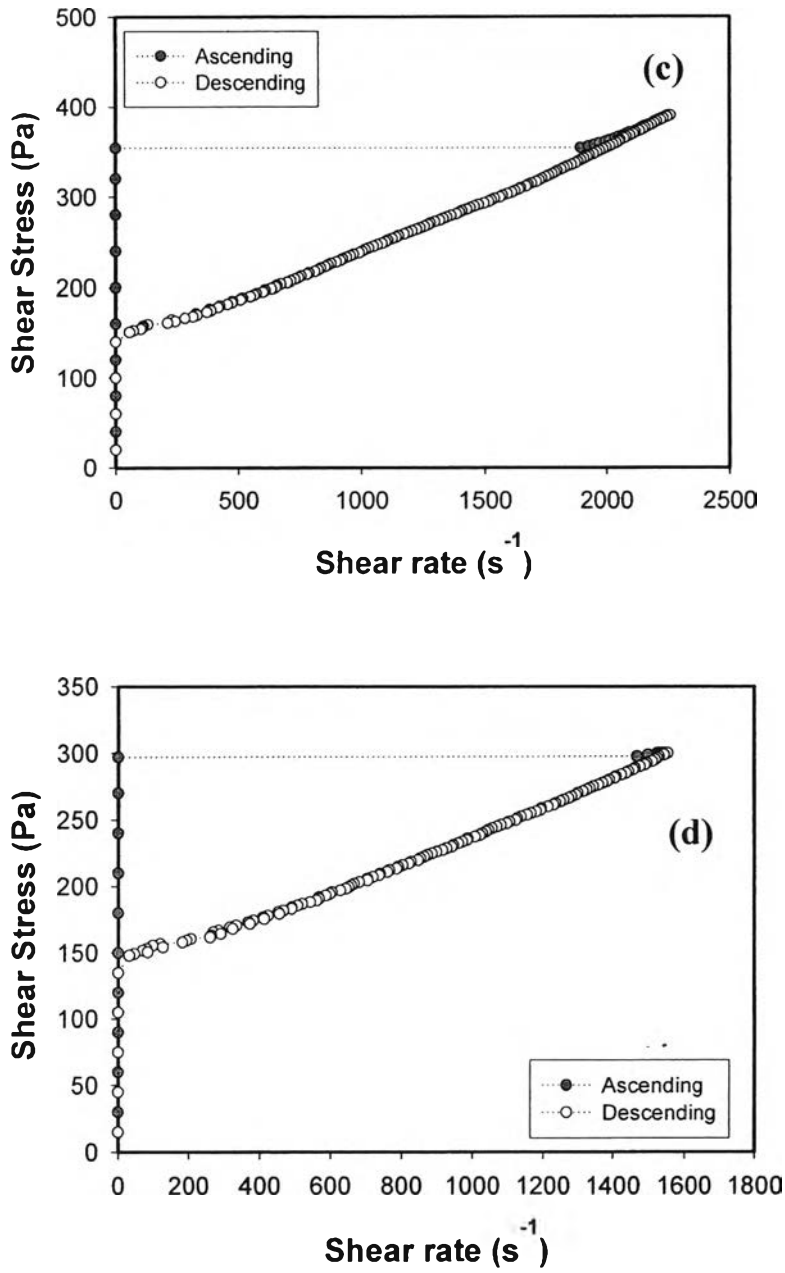

Figure 6.9 Thixotropic loop experiments performed at T = 328K (a) before shear annealing), and after shear annealing at applied stresses of (b) 110 Pa, (c) 140 Pa, and (d) 170 Pa.

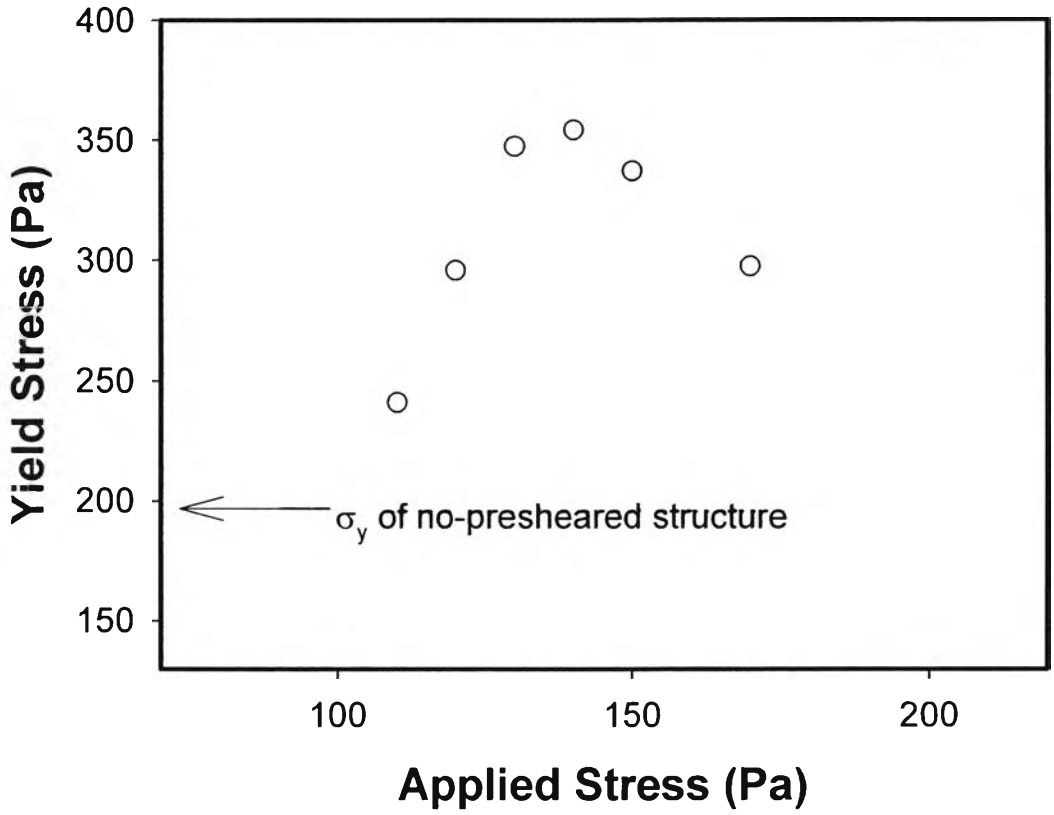

Figure 6.10 The static yield stress values measured after strain annealing at various applied stresses, measured at T = 328 K.